IN-SITU STUDY OF MATERIALS TRANSFORMATION

Thermal dynamics of P2-Na$_{0.67}$Ni$_{0.33}$Mn$_{0.67}$O$_2$ cathode materials for sodium ion batteries studied by in situ analysis

Dewen Hou[1,2], Eric Gabriel[1], Kincaid Graff[1], Tianyi Li[3], Yang Ren[4], Zihongbo Wang[1], Yuzi Liu[2,a)], Hui Xiong[1,5,a)]

[1] Micron School of Materials Science and Engineering, Boise State University, Boise, ID 83725, USA
[2] Center for Nanoscale Materials, Argonne National Laboratory, Argonne, IL 60439, USA
[3] X-Ray Science Division, Argonne National Laboratory, Argonne, IL 60439, USA
[4] Department of Physics, City University of Hong Kong, Kowloon, Hong Kong, China
[5] Center for Advanced Energy Studies, Idaho Falls, ID 83401, USA
[a)] Address all correspondence to these authors. e-mails: yuziliu@anl.gov; clairexiong@boisestate.edu

Layered Na$_{0.67}$Ni$_{0.33}$Mn$_{0.67}$O$_2$ is an attractive cathode material for sodium ion batteries. The thermal stability of cathode materials is crucial to their practical applications. In this work, we investigate structural and morphological evolution in layered P2-type Na$_{0.67}$Ni$_{0.33}$Mn$_{0.67}$O$_2$ cathode materials during annealing via in situ synchrotron X-ray diffraction and transmission electron microscopy. Insights are obtained from two complementary in situ characterizations (at different length scales) in terms of the thermal stability of P2-Na$_{0.67}$Ni$_{0.33}$Mn$_{0.67}$O$_2$ cathode materials. The results indicate that the hexagonal P2 phase remains unchanged during the heat-treatment process, and thermally driven expansion/contraction of the lattice parameters exhibits an anisotropic change in the *a* and *c* directions. In addition, interfaces/grain boundaries play an important role in the structural stability, which leads to the distinct morphological evolution between the polycrystalline and single-crystal particles.

Introduction

With the goal of reaching carbon neutrality "by or around mid-century" globally to mitigate greenhouse gas emissions, energy storage systems (EES) become pivotal for the penetration of renewable energy sources (e.g., solar and wind) as they can radically alter the way electricity is produced and consumed. As the leading technology in EES, lithium ion batteries (LIBs) have witnessed rapid development and are now ubiquitous in daily life in increasingly diverse applications ranging from portable electronics to electric vehicles [1–3]. However, the high demand on LIBs has intensified the issues associated with raw materials price as well as supply chain for critical minerals (e.g., Co and Li) [4, 5]. Various "beyond-Li" technologies are explored, among them, sodium ion batteries (SIBs) are promising due to their favorable attributes in sustainability, safety, and readiness for scaling [6–8].

Cathode materials are critical in SIBs influencing the energy, power, and cycling stability of the battery. In SIBs, transition metal oxides (TMOs), especially low-cost cobalt-free TMOs,

are the most extensively investigated cathode materials [9–13]. Many studies have hitherto focused on the development of new materials or optimization of existing materials to enhance their electrochemical performance, and attempt to explain their reaction mechanisms during cycling. However, it is equally important to investigate the thermal behaviors of cathode materials as they significantly affect the cycling stability and calendar life especially under extreme conditions. Thermal runaway might occur when a battery is overcharged or overheated, leading to fire or even explosion. Previous studies have shown that cathode materials undergo phase transformation/decomposition after cycling at high temperature [14–16]. Crystallographic changes are accompanied with oxygen release, which react with a flammable electrolyte until the thermal runaway occurs. In addition, most cathode materials are prepared by high-temperature solid-state reactions, thus observation of the thermal stability and structural transition is crucial in cathode materials synthesis [17, 18]. Finally, cathode materials with micro- or nano-size

structure exhibit unique physiochemical properties, and temperature plays an important role on the state of materials with such structure. For example, lattice parameter is a function of temperature, and the volume of cathode materials can alter in accordance with the temperature [19–21]. Further, cathode materials normally consist of numerous secondary particles formed by aggregation of smaller primary particles. During charge/discharge cycling in SIBs, it has been shown that the electrochemical performance and structural stability are strongly affected by the interface or grain boundary of primary particles of cathode materials [22–24]. However, investigations into structural evolution during annealing process are limited. There remains a lack of fundamental understanding of how temperature affects the lattice parameters and the morphology of cathode materials.

In this work, we studied the thermal behaviors of the layered P2-type $Na_{0.67}Ni_{0.33}Mn_{0.67}O_2$ (PNNMO) cathode materials during annealing in a range of temperatures (from room temperature (RT) to 700 °C). In situ high-energy synchrotron X-ray diffraction (HEXRD) experiments were performed to observe the averaged structural evolution of PNNMO materials during annealing on a global scale. Local structural and morphology changes of single-crystal and polycrystalline particles were compared through in situ transmission electron microscopy (TEM).

Results and discussion

HEXRD pattern and Rietveld refinement result of pristine PNNMO are shown in Fig. 1(a). The pristine material is composed of a hexagonal P2-layered structure as a single phase (the space group is P6$_3$/mmc). The crystallographic parameters obtained from the refinement are $a = 2.8899(7)$ Å and $c = 11.1651(6)$ Å, with $R_{wp}\% = 7.53\%$. Figure 1(b) shows a schematic diagram of the unit cell. Na atoms occupy the 2b (0, 0, 0.25) and 2d (1/3, 2/3, 0.25) sites, Ni and Mn atoms occupy the 2a site (0, 0, 0), and O atoms occupy the 4f site (2/3, 1/3, 0.1). Two particles with different microstructures (polycrystalline vs. single-crystal structure) are selected for in situ heating TEM observations. Corresponding morphologies and selected area electron diffraction (SAED) patterns from the samples at room temperature are shown in [Fig. 1(c and d)]. The size of the particles is approximately 700–800 nm. SAED patterns from both particles can be indexed as P2-type phase, which agrees with the XRD result. In addition, for the polycrystalline particle, the SAED consists of scattered diffraction spots with different crystal orientations, while for the single-crystal particle, the electron beam is parallel with [001] crystal orientation. It is noted that some weak diffraction spots can be found in the SAED pattern, implying that there are small portions of regions that have different orientations, which will be discussed later.

Figure 2 shows the in situ HEXRD/heating results (left panel) and evolution of lattice spacing (right panel) as a function of temperature (the temperature range RT to 750 °C). It is evident that the pristine PNNMO sample is thermally stable up to 750 °C, as no decomposition of the initial phase/generation or new phase occurs during heating–holding–cooling processes. According to the Rietveld refinement results, the lattice parameters a and c manifest expansion/contraction upon heating/cooling, and no significant change is observed during holding process. Lattice parameter a swells from 2.8899 Å (RT) to 2.9114 Å (750 °C) with the expansion of ~ 0.73% ($\Delta a/a$), while lattice c swells from 11.1651 Å (RT) to 11.3003 Å (750 °C) with an expansion of 1.19% ($\Delta c/c$). Meanwhile, the unit cell volume (V) swells from 80.7579 Å^3 (RT) to 82.8905 Å^3 (750 °C) with the expansion of 2.64% ($\Delta V/V$). Here, Δa, Δc, and ΔV are the change in lattice parameter at different temperatures (i.e., $\Delta a = a_{750°C} - a_{RT}$, $\Delta c = c_{750°C} - c_{RT}$), and $\Delta V = V_{750°C} - V_{RT}$. It is noted that from 200 to 300 °C, the expansion of lattice c is relatively small, as indicated by the plateau in c/a. During the cooling process, both a and c shrink rapidly and eventually reduce to close to their initial values (2.8902 Å and 11.1680 Å), implying that the change in lattice parameters is reversible after annealing. Although the lattice parameters vary with temperature in both the a and c directions, their dependence on temperature suggests an anisotropic characteristic. As shown in the evolution of c/a, the ratio increases with increasing temperature and reaches a maximum at 750 °C, above which it decreases gradually. It means that the thermal expansion along c direction is larger than a direction. The material electrochemical performance might benefit from such anisotropic properties since the Na would intercalate between layers stacking along c direction.

For the polycrystalline PNNMO particle sample, the secondary particle is composed of many primary grains with different orientations. Temperature-dependent changes in the morphology and crystal structure of the polycrystalline PNNMO particle were recorded by a series of bright-field micrographs and corresponding SAED patterns, as shown in Fig. 3. When temperature increases from RT to 300 °C, no clear structural change is observed in the sample. This implies that the structure of the polycrystalline particle is thermally stable below 300 °C, despite the slight expansion of the lattice parameters. Between 400 and 600 °C, obvious structural changes and some surface roughening are observed. Some new and weak diffraction spots start appearing at 400 °C. As the temperature rises, increasing numbers of new spots are shown, with a subsequent evolution of SAED patterns towards diffraction rings. These new diffraction spots indicate the formation of new nano-grains during the heating process.

In previous reports, the evolution of diffraction patterns from single-crystal spots to polycrystalline rings is mainly due to the phase transformation of materials upon heating [14, 16].
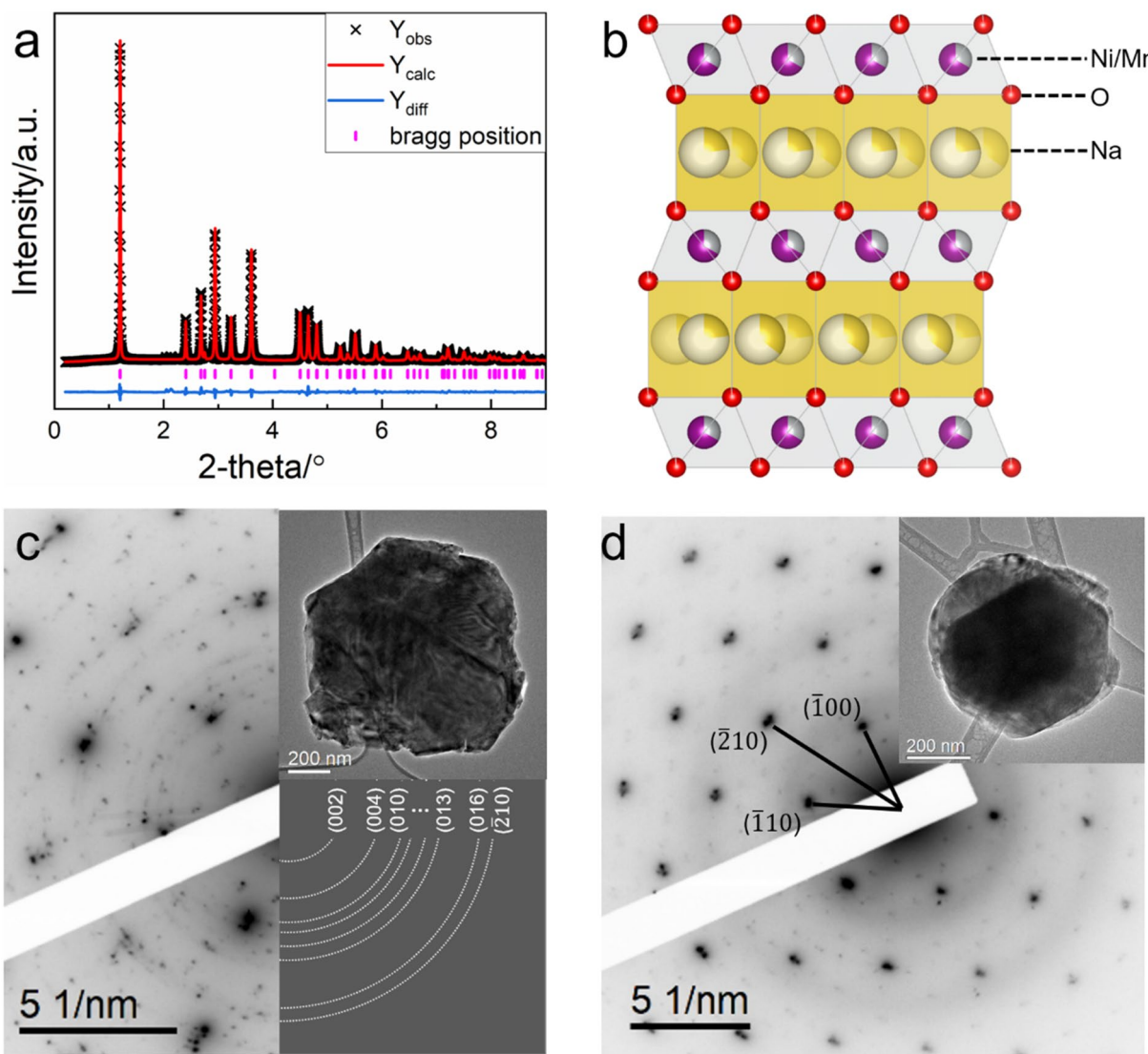
Figure 1: (a) HEXRD and Rietveld refinement results of pristine PNNMO. (b) Schematic diagram of the unit cell. TEM results of two particles with (c) polycrystalline structure and (d) single-crystal structure.

In this work, the materials have no phase transformation during heating process. Thus, it can be concluded that one important driving force for the new nano-grains is the accumulation of internal strain caused by thermal expansion of the crystal lattice.

In a well-crystallized polycrystalline particle, a large number of primary particles have non-regular geometry and different lattice orientations, and any two of them are connected by a shared interface. As the temperature increases, the lattice parameters of the material undergo expansion in both a and c directions (Fig. 2). These expansions will exert internal stresses to the primary particles. Due to the combined effect of interface and misorientations between two primary grains, the internal stress will gradually accumulate. When the stress reaches a critical value, defects or even nano-grains will be generated within primary particles due to large strain. This phenomenon was

observed by HRTEM. Figure 4 shows local structural evolution at the same position, before and after annealing. Compared to the initial structure, the sample after heat-treatment exhibits a significant concentration of defects with the crystal orientation change.

At 700 °C, the particle mostly maintains its initial shape, but the thickness contours become weak over the entire area. In addition, the diffraction rings formed during 400–600 °C become intermittent (some new diffraction spots disappear), indicating that partial nano-grains merge with each other or primary grains. During the subsequent temperature reduction, as shown in Fig. 3, the morphologies and structures of the particle do not change significantly, which means the particle is stable during cooling process.
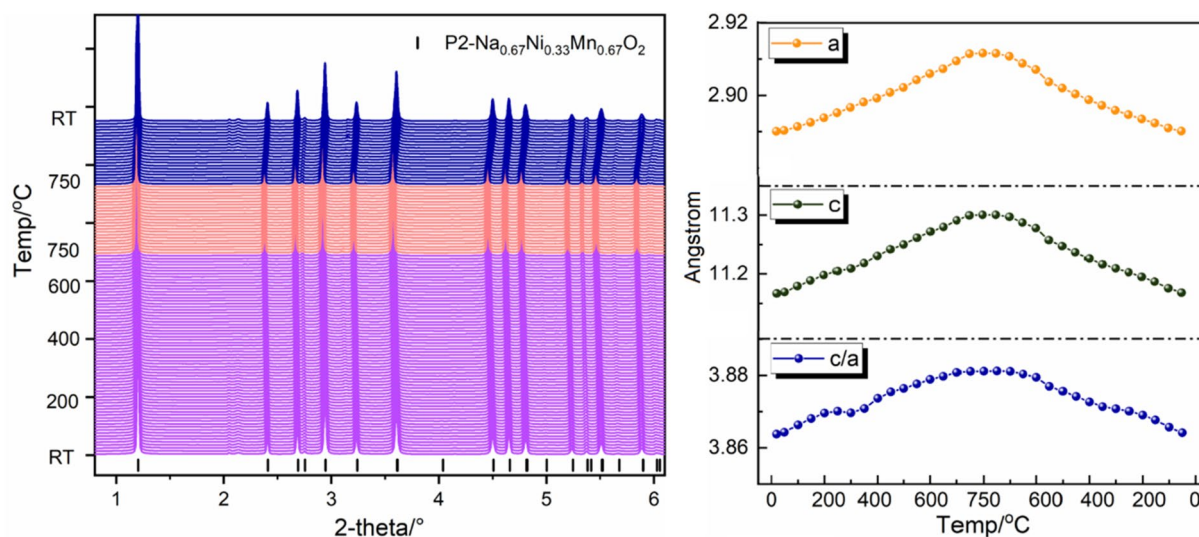
Figure 2: In situ HEXRD evolution of pristine PNNMO cathode during heating–warming–cooling processes (left panel), and corresponding lattice parameters evolution (right panel). The sample was held at 750 °C for 10 min.
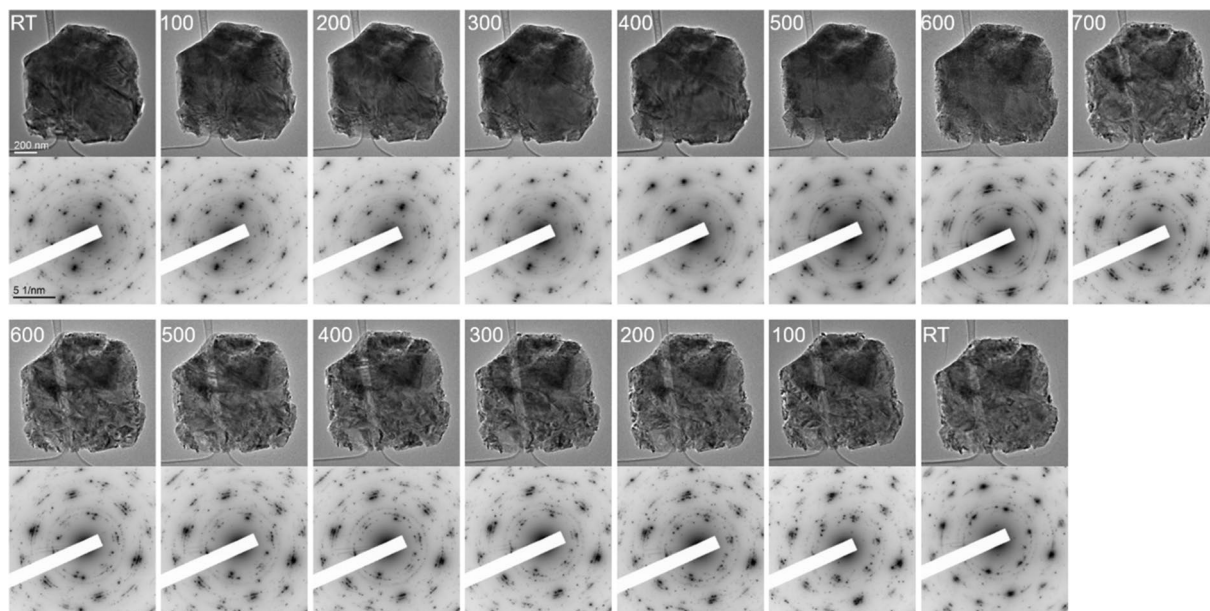

Figure 3: Real-time bright-field images and SAED patterns of the polycrystalline PNNMO particle at different temperatures.

For the single-crystal PNNMO particle sample, the particle exhibits a preferred orientation, i.e., most areas of the particle have a homogenous crystal orientation. As shown in Figs. 1(c) and 5, the initial particle has a preferred orientation with [001] zone axis. Meanwhile, a few weak diffraction spots can be found in the SAED pattern at RT, which implies that a small portion of the regions are oriented differently from the [001] zone axis. These regions are mainly located on the edge of the particle (Fig. 6). Therefore, for the current work, we assume that the particle has a single-crystal structure.

Figure 5 shows a sequence of bright-field images and SAED patterns of single-crystal particle during in situ TEM/annealing. The morphology and structure of the particles are maintained upon heating to 300 °C, which is in agreement with the structural evolution of the polycrystalline particle. Two weak halo rings are found in the SAED pattern at RT, and their intensities increase as the temperature rises. These halo rings are from the amorphous carbon support films. At high temperature, the amorphous carbon converts to a polycrystalline structure, as presented by shaper rings in the diffraction patterns [25]. In
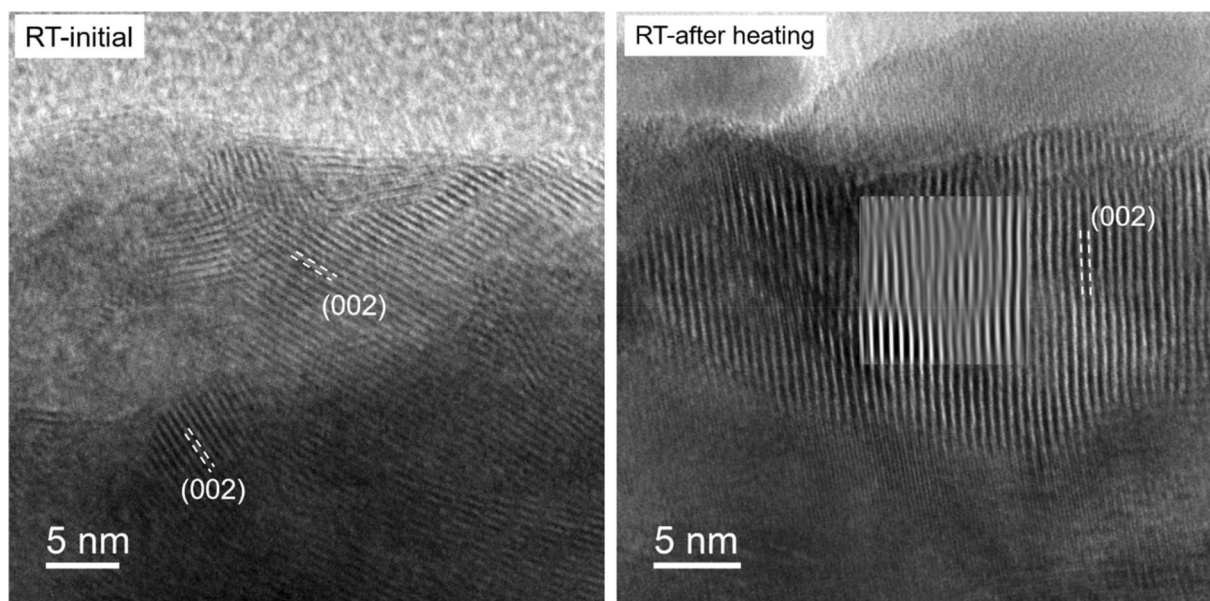
Figure 4: HRTEM images of the polycrystalline structure particle at RT: before (left) and after (right) annealing. The structural disordering after annealing is highlighted by inserted inverse fast Fourier transform (IFFT).
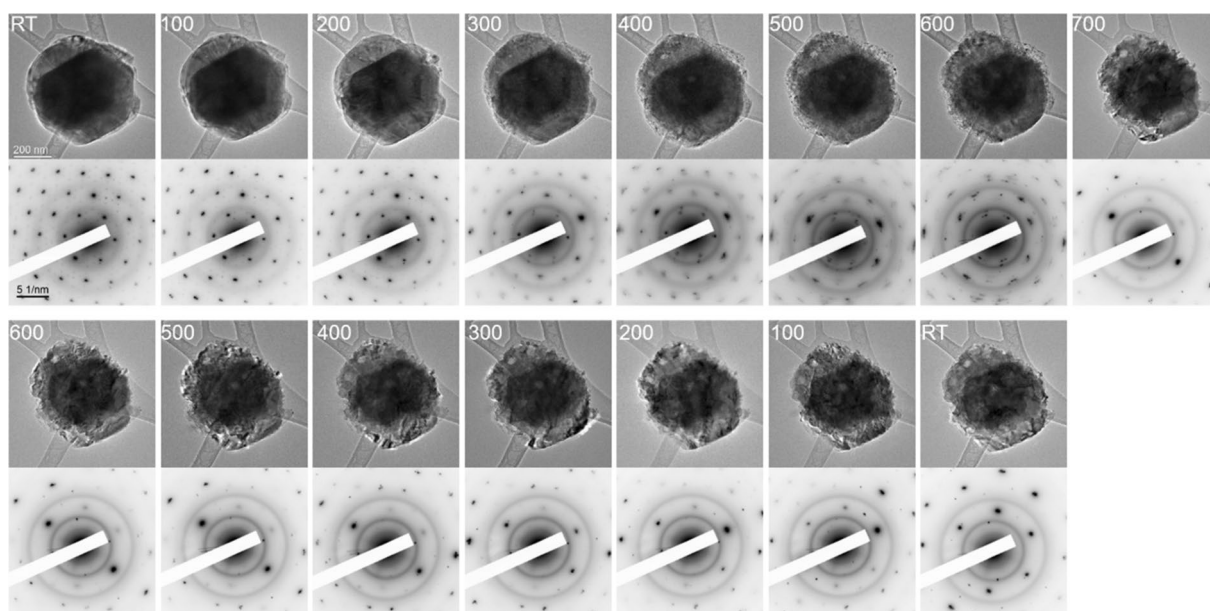

Figure 5: Real-time bright-field images and SAED patterns of the single-crystal PNNMO particle at different temperatures.

addition, due to the rotation of sample upon heating, the particle orientation deviates from the [001] zone axis, resulting in the intensities of partial diffraction spots weakening at 300 °C.

As the temperature continues to rise from 400 to 600 °C, serious surface roughening and slight volume expansion are observed. No additional diffraction spots are present (i.e., no nano-grains form during heating), which is in contrast to the polycrystalline particle. This difference mainly comes from

the influence of the interfaces or grain boundaries among primary grains. As mentioned above, crystal lattices will expand as a result of heating, which in turn generates strain inside the primary grains. For the polycrystalline particle, these strains accumulate gradually due to restriction by interfaces/grain boundaries between different primary particles, resulting in formation defects or even nano-grains. For the single-crystal particle, there is no interface to prevent internal strain, resulting
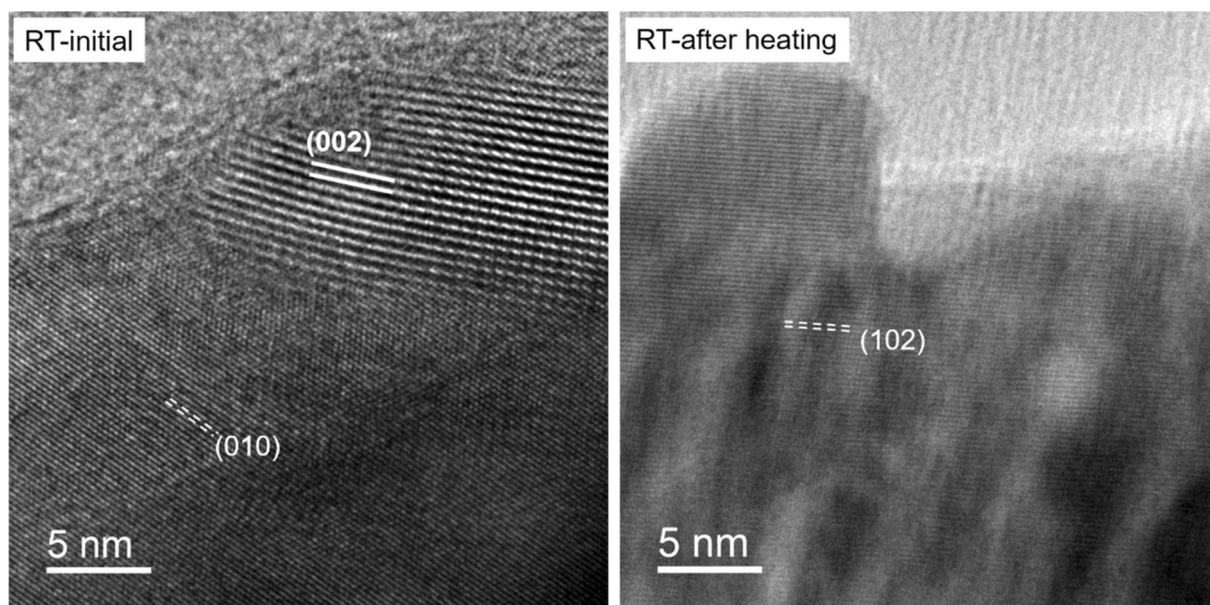
Figure 6: HRTEM analysis of the single-crystal PNNMO particle at RT: before (left panel) and after (right panel) annealing. High-magnification images taken from the same local surface area.

in homogeneous thermal expansion that occurs throughout the particle accompanied by the expansion of the lattice (regardless of the lattice expansion being isotropic or anisotropic). This difference can also be observed by local regional evolution (before and after annealing), as shown by HRTEM images in Figs. 4 and 6.

Due to the lack of effect by interface/grain boundaries, the volume of the single-crystal particle undergoes a violent shrinking when the temperature reaches 700 °C. Meanwhile, no new diffraction spots are observed, and the entire particle maintains a single-crystal structure. The particle does change noticeably during subsequent cooling processes, which is in agreement with the structural evolution of the polycrystalline particle.

Conclusions

In conclusion, we used in situ HEXRD and in situ TEM to investigate the thermal behaviors of pristine PNNMO cathode materials for SIBs. The combination of the two in situ measurements at different length scales provides a detailed picture of thermal behaviors which occur in the PNNMO materials. The conclusions are summarized as follows: (1) no phase transformation occurs during annealing process up to 750 °C; (2) thermally driven expansion/contraction of lattice parameters exhibit an anisotropic character in the *a* and *c* directions; (3) the edges of the particles become more fractured as the temperature increases, but overall particle morphology maintains below 700 °C; (4) interfaces/grain boundaries lead to new nano-grains

formation due to internal strain accumulation within primary particles.

Methods

The pristine PNNMO cathode materials were prepared by high-temperature solid-state reactions adopted from previous work [26].

In situ HEXRD/annealing experiments were performed at sector 11-ID-C of Advanced Photon Source (APS) in the Argonne National Laboratory. The wavelength of the X-ray is 0.1173 Å. Annealing tests were carried out by using a Linkam heating stage (Model TS1500). The furnace has a tolerance of 50 °C. To avoid contact between the samples and air, argon was used as a protective atmosphere during the annealing process. The cathode PNNMO materials were first heated from RT to 750 °C at 20 °C /min, then held at 750 °C for 10 min. After that, the sample was cooled down to RT. The 2D diffraction patterns were calibrated by a standard CeO_2 sample and converted to 1D diffraction patterns by GSAS II software. The in situ structural change and lattice parameter evolution were monitored using Rietveld refinement with GSAS II program [27].

In situ TEM/annealing tests were carried out in a JEOL JEM2100F microscope. The working voltage is 200 kV. A Gatan double tilt heating holder (Model 652-Ta) was used for in situ annealing. The temperature was controlled using the Gatan Temperature Controller (Model 1905). For each sample's preparation, the powder was first dropped on an Au grid coated with an amorphous carbon support film in the glovebox, then quickly transferred to the heating holder. To reduce the high-energy

electron beam effect, the beam valve was open only during image recording. To minimize thermal drift and ensure the sample reaches the target temperature, image recording was started after temperature stability.

Acknowledgments

Data availability

The datasets generated during and/or analyzed during the current study are available from the corresponding author on reasonable request.

Declarations

Conflict of interest The authors declare that they have no known competing financial interests or personal relationship that could have appeared to influence the work reported in this paper.

References

1. E. Pomerantseva, F. Bonaccorso, X. Feng, Y. Cui, Y. Gogotsi, Energy storage: the future enabled by nanomaterials. Science **366**(6468), eaan8285 (2019)

2. S. Chu, A. Majumdar, Opportunities and challenges for a sustainable energy future. Nature **488**(7411), 294 (2012)

3. M. Li, J. Lu, Z. Chen, K. Amine, 30 years of lithium-ion batteries. Adv. Mater. **30**(33), 1800561 (2018)

4. C. Vaalma, D. Buchholz, M. Weil, S. Passerini, A cost and resource analysis of sodium-ion batteries. Nat Rev Mater **3**(4), 18013 (2018)

5. J. M. Granholm. National blueprint for lithium batteries 2021-2030. **24** (2021)

6. T. Hosaka, K. Kubota, A.S. Hameed, S. Komaba, Research development on K-ion batteries. Chem. Rev. **120**(14), 6358 (2020)

7. M.D. Slater, D. Kim, E. Lee, C.S. Johnson, Sodium-ion batteries. Adv. Func. Mater. **23**(8), 947 (2013)

8. S. Komaba, Sodium-driven rechargeable batteries: an effort towards future energy storage. Chem. Lett. **49**(12), 1507 (2020)

9. S. Chu, S. Guo, H. Zhou. Advanced cobalt-free cathode materials for sodium-ion batteries. Chem. Soc. Rev. (2021)

10. J. Alvarado, C. Ma, S. Wang, K. Nguyen, M. Kodur, Y.S. Meng, Improvement of the cathode electrolyte interphase on P2-Na2/3Ni1/3Mn2/3O2 by atomic layer deposition. ACS Appl. Mater. Interfaces **9**(31), 26518 (2017)

11. C. Deng, P. Skinner, Y. Liu, M. Sun, W. Tong, C. Ma, M.L. Lau, R. Hunt, P. Barnes, J. Xu, H. Xiong, Li-substituted layered spinel cathode material for sodium ion batteries. Chem. Mater. **30**(22), 8145 (2018)

12. C. Deng, E. Gabriel, P. Skinner, S. Lee, P. Barnes, C. Ma, J. Gim, M.L. Lau, E. Lee, H. Xiong, Origins of irreversibility in layered NaNixFeyMnzO2 cathode materials for sodium ion batteries. ACS Appl. Mater. Interfaces **12**(46), 51397 (2020)

13. D. Hou, D. Xia, E. Gabriel, J. A. Russell, K. Graff, Y. Ren, C.-J. Sun, F. Lin, Y. Liu, H. Xiong. Spatial and temporal analysis of sodium-ion batteries. ACS Energy Lett. **4023** (2021)

14. N. Yabuuchi, I. Ikeuchi, K. Kubota, S. Komaba, Thermal stability of NaxCrO2 for rechargeable sodium batteries; studies by high-temperature synchrotron x-ray diffraction. ACS Appl. Mater. Interfaces **8**(47), 32292 (2016)

15. C. Yang, S. Xin, L. Mai, Y. You, Materials design for high-safety sodium-ion battery. Adv. Energy Mater. **11**(2), 2000974 (2021)

16. S. Hwang, Y. Lee, E. Jo, K.Y. Chung, W. Choi, S.M. Kim, W. Chang, Investigation of thermal stability of P2–Na$_x$CoO$_2$ cathode materials for sodium ion batteries using real-time electron microscopy. ACS Appl. Mater. Interfaces **9**(22), 18883 (2017)

17. T. Ma, G.-L. Xu, X. Zeng, Y. Li, Y. Ren, C. Sun, S.M. Heald, J. Jorne, K. Amine, Z. Chen, Solid state synthesis of layered sodium manganese oxide for sodium-ion battery by in-situ high energy X-ray diffraction and X-ray absorption near edge spectroscopy. J. Power Sources **341**, 114 (2017)

18. X.-B. Zhong, C. He, F. Gao, Z.-Q. Tian, J.-F. Li, In situ Raman spectroscopy reveals the mechanism of titanium substitution in P2–Na2/3Ni1/3Mn2/3O2: cathode materials for sodium batteries. J. Energy Chem. **53**, 323 (2021)

19. V. Baran, O. Dolotko, M.J. Mühlbauer, A. Senyshyn, H. Ehrenberg, Thermal structural behavior of electrodes in li-ion battery studied in operando. J. Electrochem. Soc. **165**(9), A1975 (2018)

20. W. Kobayashi, A. Yanagita, T. Akaba, T. Shimono, D. Tanabe, Y. Moritomo, Thermal expansion in layered Na × MO$_2$. Sci Rep **8**(1), 3988 (2018)

21. A.K. Bera, S.M. Yusuf, Temperature-dependent na-ion conduction and its pathways in the crystal structure of the layered battery material Na$_2$Ni$_2$TeO$_6$. J. Phys. Chem. C **124**(8), 4421 (2020)

22. S. Guo, Q. Li, P. Liu, M. Chen, H. Zhou, Environmentally stable interface of layered oxide cathodes for sodium-ion batteries. Nat Commun **8**(1), 135 (2017)

23. Y. Huang, L. Zhao, L. Li, M. Xie, F. Wu, R. Chen, Electrolytes and electrolyte/electrode interfaces in sodium-ion batteries: from scientific research to practical application. Adv. Mater. **31**(21), 1808393 (2019)

24. T.-Y. Yu, H.-H. Ryu, G. Han, Y.-K. Sun, Understanding the capacity fading mechanisms of O$_3$-Type Na[Ni$_{0.5}$Mn$_{0.5}$]O$_2$

cathode for sodium-ion batteries. Adv. Energy Mater. **10**(37), 2001609 (2020)

25. Z. Huang, Y. Yao, Z. Pang, Y. Yuan, T. Li, K. He, X. Hu, J. Cheng, W. Yao, Y. Liu, A. Nie, S. Sharifi-Asl, M. Cheng, B. Song, K. Amine, J. Lu, T. Li, L. Hu, R. Shahbazian-Yassar, Direct observation of the formation and stabilization of metallic nanoparticles on carbon supports. Nat. Commun. **11**(1), 6373 (2020)

26. Y. Xie, E. Gabriel, L. Fan, I. Hwang, X. Li, H. Zhu, Y. Ren, C. Sun, J. Pipkin, M. Dustin, M. Li, Z. Chen, E. Lee, H. Xiong, Role of lithium doping in P2-$Na_{0.67}Ni_{0.33}Mn_{0.67}O_2$ for sodium-ion batteries. Chem. Mater. **33**(12), 4445 (2021)

27. B.H. Toby, R.B. Von Dreele, GSAS-II: the genesis of a modern open-source all purpose crystallography software package. J. Appl. Cryst. **46**(2), 544 (2013)